RESEARCH ARTICLE

Assembling hexagonal-bipyramidal {Mn_8Zn_2} and {Mn_8Zn_4} clusters

Thomais G. Tziotzi,[a] Evangelos K. Andreou,[a] Athanasios Mavromagoulos,[b] Mark Murrie,[b] Scott J. Dalgarno,[c] Euan K. Brechin,*[d] and Constantinos J. Milios*[a]

[a] Dr. T.G. Tziotzi, Mr. E. K. Andreou, Dr. Prof. C. J. Milios
Department of Chemistry
University of Crete
Voutes Campus, 71003, Herakleion, Greece
E-mail: komil@uoc.gr
[b] Mr. A. Mavromagoulos, Dr. Prof. M. Murrie,
School of Chemistry
University of Glasgow
University Avenue, Glasgow, G12 8QQ, UK
[c] Dr. S. J. Dalgarno
Institute of Chemical Sciences
Heriot-Watt University
Riccarton, Edinburgh, Scotland, EH14 4AS, UK
[d] Dr. Prof. E. K. Brechin
EaStCHEM School of Chemistry
The University of Edinburgh
David Brewster Road, Edinburgh, EH9 3FJ, UK
E-mail: ebrechin@ed.ac.uk

Supporting information for this article is given via a link at the end of the document.

Abstract: Reaction between $Mn(NO_3)_2{\cdot}6H_2O$, $Zn(NO_3)_2{\cdot}6H_2O$, 1,3,5-tri(2-hydroxyethyl)-1,3,5-triazacyclohexane (H_3L) and pyrazole in MeOH under basic conditions leads to the formation of the decanuclear complex $[Mn^{III}_6Mn^{II}_2Zn^{II}_2(L)_2(pyr)_4O_4(OH)_4(NO_3)_2(MeOH)_2(H_2O)_4](NO_3)_2{\cdot}H_2O$ (**1**·H_2O). The metallic core of the cationic cluster consists of a central hexagonal-bipyramidal $\{Mn^{III}_4Mn^{II}_2Zn^{II}_2\}$ unit connected to two peripheral trivalent Mn centers arranged in a "*trans*" fashion, with one Mn^{III} center lying above and one Mn^{III} center below the hexagonal plane. Replacing $Mn(NO_3)_2{\cdot}6H_2O$ with $MnBr_2{\cdot}4H_2O$ and repeating the same reaction leads to the formation of the related, neutral decanuclear complex $[Mn^{III}_6Mn^{II}_2Zn^{II}_2(L)_2(pyr)_4O_4(OH)_4Br_4(H_2O)_2]$ (**2**), displaying the same metallic core as **1**. Addition of THF to the reaction mixture that produces (**2**) affords the neutral dodecanuclear complex $[Mn^{III}_6Mn^{II}_2Zn^{II}_4(L)_2(pyr)_6O_4(OH)_4Br_6(H_2O)_4]{\cdot}8THF$ (**3**·8THF) whose metallic skeleton retains the central hexagonal-bipyramidal $\{Mn^{III}_4Mn^{II}_2Zn^{II}_2\}$ unit found in **1** and **2**, but is now connected to two peripheral $\{Mn^{III}Zn^{II}\}$ units. Magnetic susceptibility and magnetization measurements carried out in the T = 2 – 300 K temperature range and in fields up to B = 7.0 T for all three complexes reveal dominant antiferromagnetic exchange interactions.

Introduction

Despite the success of N,O-chelate type ligands for the synthesis of polymetallic clusters of paramagnetic 3d cages,[1] a search of the Cambridge Structural Database (CSD) for the pro-ligand 1,3,5-tri(2-hydroxyethyl)-1,3,5-triazacyclohexane (LH_3; Figure 1) reveals just five hits. The first reported example,[2] in 1999, was the monomer $[Cr(CO)_3(LH_3)]$ and the second, in 2019, an aesthetically pleasing torus-like $[Mn_{16}]$ complex,[3] in which the ligand was generated serendipitously *in situ*. This was followed more recently by a $[Mn_{16}]$ double square wheel,[4] a $[Mn_{10}]$ contorted wheel,[4] and an $[Mn_{18}]$ wheel of wheels.[5] Despite there being only four examples in Mn chemistry a trend in the mode of action of the deprotonated ligand (L^{3-}, LH^{2-}) is becoming apparent. The ligand assembles an oxo-centered triangle $[Mn^{III}_3O(LH_x)]^{y+}$ (x = 0,1; y = 4, 5) in which the triaza N-atoms are coordinated to the Jahn-Teller (JT) axes of the Mn^{III} ions, *i.e.* the JT axes are co-parallel, lying perpendicular to the $[Mn_3O]$ plane (Figure 1). This moiety has several interesting features: (a) paramagnetic metal ions arranged into triangles can show magnetic frustration effects which can lead to some interesting, and potentially useful, low temperature physics;[6] (b) a parallel arrangement of JT axes is beneficial to the manufacture of single-molecule magnets;[7] (c) control over the orientation of JT axes allows control over both the magnetic anisotropy of the cluster complex, and control over the nature of magnetic exchange (ferromagnetic/antiferromagnetic) interaction between nearest neighbours.[8-10] The self-assembly of these triangular moieties *via* the bridging O-atoms of the ligand therefore has the potential to produce a large number of novel structures, with the physical characterisation of families of related species allowing detailed, quantitative magneto-structural correlations. Given that there are only five complexes known, and all are in Mn or Cr chemistry, one may also assume that a vast number of complexes of other 3d metals with this ligand remain undiscovered.

Herein, we extend the coordination chemistry of LH_3 by reporting the synthesis, structures and magnetic properties of $[Mn^{III}_6Mn^{II}_2Zn^{II}_2(L)_2(pyr)_4O_4(OH)_4(NO_3)_2(MeOH)_2(H_2O)_4](NO_3)_2{\cdot}H_2O$ (**1**·H_2O), $[Mn^{III}_6Mn^{II}_2Zn^{II}_2(L)_2(pyr)_4O_4(OH)_4Br_4(H_2O)_2]$ (**2**) and $[Mn^{III}_6Mn^{II}_2Zn^{II}_4(L)_2(pyr)_6O_4(OH)_4Br_6(H_2O)_4]{\cdot}8THF$ (**3**·8THF) all of

which have structures based on hexagonal bipyramids and which both extend the family of known Mn clusters and represent the first examples of heterometallic clusters.

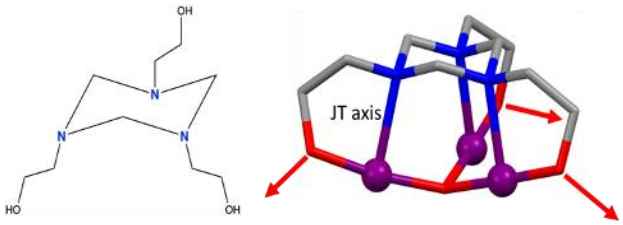

Figure 1. (Left) The ligand 1,3,5-tri(2-hydroxyethyl)-1,3,5-triazacyclohexane (LH_3). (Right) The bonding mode solely observed for L^{3-}/LH^{2-} in Mn chemistry, forming a $[Mn^{III}_3O(LH_x)]^{y-}$ (x = 0,1; y = 4, 5) moiety. The triaza N-atoms of the ligand are bonded to the JT sites on Mn^{III}, perpendicular to the $[Mn_3]$ plane, with the O-atoms further bridging to additional metal ions. Colour code: Mn^{III} = purple, O = red, N = blue, C= grey. H atoms omitted for clarity.

Results and Discussion

The equimolar reaction between $Mn(NO_3)_2{\cdot}6H_2O$, $Zn(NO_3)_3{\cdot}6H_2O$, pyrazole and LH_3 in the presence of base, NEt_3, in MeOH forms the cationic decanuclear complex $[Mn^{III}_6Mn^{II}_2Zn^{II}_2(L)_2(pyr)_4O_4(OH)_4(NO_3)_2(MeOH)_2(H_2O)_4](NO_3)_2{\cdot}H_2O$ (**1**$\cdot H_2O$), in good yield. The cluster is mixed-valent containing six Mn^{III} and two Mn^{II} centers, despite the fact that the starting material contained exclusively divalent manganese ions. The oxidation process is attributed to base-assisted aerial oxidation. Changing synthetic parameters, *i.e.* metal-to-ligand ratios, reaction times and nature of the base, does not lead to the formation of new products as evidenced by PXRD and IR comparisons. Furthermore, attempts to increase the Zn content of the cluster proved unsuccessful - all Mn:Zn ratios employed up to a ratio of 1:3 produced complex **1** as the sole product of the reaction. This points toward the predisposition of the LH_3 ligand for trivalent metals, as reflected by the crystal structures of all three complexes reported herein (*vide infra*). Therefore, we changed the Mn salt to $MnBr_2{\cdot}4H_2O$ as a means of replacing the labile nitrate ions with bulky bromides in order to change the identity of the product. The result was the isolation of the neutral decanuclear complex $[Mn^{III}_6Mn^{II}_2Zn^{II}_2(L)_2(pyr)_4O_4(OH)_4Br_4(H_2O)_2]$ (**2**) which displays the same main structural features as **1**, with the difference now being the replacement of the two monodentate nitrate ions and two terminal H_2O molecules in **1** with four terminal Br^- ions in **2**, thus establishing **2** as the "charge-isomer" of the former complex. Switching to a less polar environment by using an equimolar MeOH/THF solvent mixture resulted in an increase in the nuclearity of the product obtained in the form of the neutral dodecanuclear complex $[Mn^{III}_6Mn^{II}_2Zn^{II}_4(L)_2(pyr)_6O_4(OH)_4Br_6(H_2O)_4]{\cdot}8THF$ (**3**$\cdot$8THF). The mixed-valent $\{Mn^{III}_6Mn^{II}_2\}$ oxidation state observed in (**1**) and (**2**) is retained in (**3**), but the Zn content has doubled.

A detailed search of the CSD revealed just eighteen hits for O-bridged heterometallic {Mn/Zn} clusters. Of these, four are dimers, four are trimers and five are tetramers.[11-16] Complexes **1** and **2** are the first examples of decanuclear species and complex **3** the first dodecanuclear {Mn/Zn} cluster. Furthermore, if the search is widened to include any bridging atoms complexes **1**-**3** are rare examples of large polynuclear {Mn/Zn} species, with only two examples of larger nuclearity clusters having been reported: an impressive $\{Mn_{12}Zn_{24}\}$ chiral metallosalen-based octahedral cage,[17] and a family of ternary $\{Zn_{14-x}Mn_xS_{13}/Se_{13}Cl_2(tmeda)_6\}$ clusters (tmeda = N,N,N′,N′-tetramethylethylenediamine; x~ 2-8). Complex **1** crystallizes in the monoclinic space group *C2/c*. Its metallic core (Figure 2) describes a central hexagonal-bipyramidal $\{Mn^{III}_4Mn^{II}_2Zn^{II}_2\}$ unit linked to two peripheral trivalent manganese centers in a "*trans*" orientation with respect to the hexagonal plane. The edges of the hexagon fall in the 2.80-3.17 Å range, with four of its vertices being Mn^{III} ions (Mn1, Mn3 and symmetry equivalent (s.e)) and the remaining two occupied by Mn^{II} ions (Mn4 and s.e). Mn-O-Mn bond angles all fall in the range ~111-125º with the smaller angles associated with the divalent Mn centers. The apical positions of the hexagonal-bipyramidal unit are occupied by the two Zn ions, located ~1.6 Å above and below the hexagonal plane, and are slightly off-set from each other (O-Mn-Mn, ~170 º). The peripheral Mn^{III} ions (Mn2 and s.e) are located at each side of the central unit ~1.3 Å above and below the hexagonal plane, respectively. The assembly of the dodecametallic skeleton occurs *via*: i) four deprotonated arms belonging to the two L^{3-} ligands, serving as monoatomic μ-bridges between the basal divalent and trivalent Mn ions, ii) two μ_3-O^{2-} bridges (O5/O5') responsible for bridging the peripheral Mn ions (Mn2 and s.e) to the Mn1-Mn3 (and s.e) edge of the hexagon, iii) two μ_3-O^{2-} bridges (O4/O4') responsible for bridging the apical Zn ions to the Mn1-Mn3 (and s.e) edge of the hexagon, and iii) four μ_3-OH^- bridges (O11, O13 and s.e) responsible for holding the apical Zn ions to the Mn-Mn4 (and s.e) and Mn3-Mn4 (and s.e) edges of the base. The two ligands are found in their fully deprotonated form, L^{3-}, each capping three Mn^{III} ions (Mn1, Mn2, Mn3 and s.e) belonging to an oxo-centered $\{Mn_3O\}$ triangle *via* coordination of their N-atoms to the Jahn-Teller (JT) sites on the Mn^{III} ions, perpendicular to the $[Mn_3]$ plane, adopting an overall η^2: η^2: η^1: η^1: η^1: μ_5-coordination mode. The four pyrazolate ligands found in the complex adopt their usual η^1: η^1: μ-coordination mode. The coordination environments of the metal ions are completed by the presence of: i) one methanol molecule on Mn2 (and s.e), ii) one monodentate nitrate ion and one H_2O molecule on Mn4 (and s.e), and iii) one H_2O molecule on each Zn ion. The assignment of the Mn oxidation states was performed on the basis of BVS calculations (Table S2) and the presence of JT axes for the six-coordinate Mn^{III} ions. All the Mn ions are six-coordinate, while the Zn^{II} ions are four-coordinate adopting tetrahedral geometry. In the crystal lattice, the molecules pack forming chains along the *b* axis (Fig. S1), with the most significant intermolecular interactions being H-bonds formed between the nitrate counter anions and the terminal H_2O molecules on the Zn ions of neighboring decanuclear species (~2.6-2.9 Å), responsible for connecting neighboring chains.

The metallic skeleton and overall molecular structure of $[Mn^{III}_6Mn^{II}_2Zn^{II}_2(L)_2(pyr)_4O_4(OH)_4Br_4(H_2O)_2]$ (**2**) (Figure 3) is very similar to **1**, so we highlight just the major structural differences between these two molecules: i) The monodentate nitrate ion and the terminal H_2O molecule coordinated to each Mn^{II} ions of **1** have been replaced by one terminal Br^- ion in **2** (Mn4 and s.e.), and ii) the terminal H_2O molecule on each Zn ion of **1** has now been replaced by a terminal Br^- in **2**. Therefore, Mn4 (and s.e) is now five-coordinate (*vs*. six-coordinate in **1**) adopting square-pyramidal geometry (τ = 0.021), while the remaining Mn ions are all six-coordinate. All Zn ions are tetrahedral. The mixed-valent

$\{Mn^{III}_6Mn^{II}_2\}$ oxidation state was verified by both BVS calculations (Table S2) and the expected elongated JT distortion for the trivalent Mn centers. **2** is neutral as opposed to the dicationic cluster in **1**. In the crystal lattice, **2** form chains *via* H-bond formation between neighbouring clusters: each molecule forms four H-bonds to two adjacent molecules through the terminal H_2O molecule on Mn2 (and s.e.) and the monodentate deprotonated arm of each L^{3-} ligand (O(H)···O, ~2.6 Å).

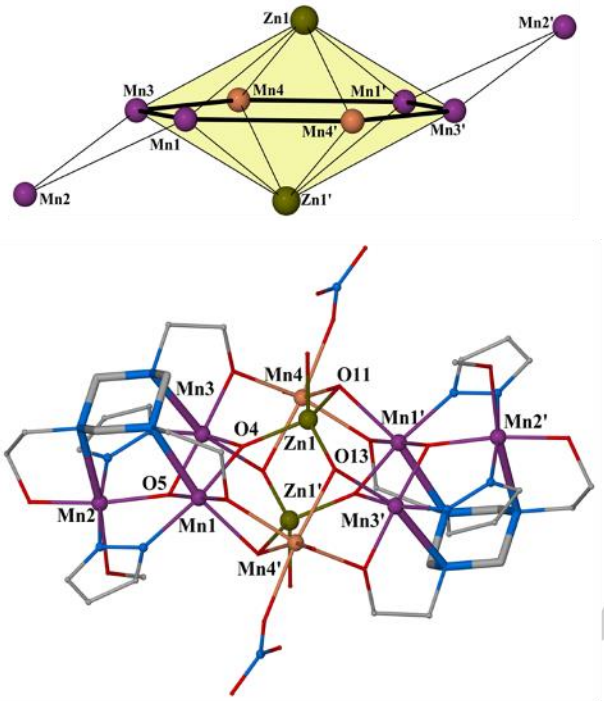

Figure 2. (Top) The metallic skeleton of **1**, with the highlighted section showing the hexagonal bipyramidal core. (Bottom) The molecular structure of the dication of **1**, highlighting the capping mode of the triaza N-atoms on the JT sites of Mn^{III} ions. Colour code: Mn^{III} = purple, Mn^{II} = orange, Zn= grey-green, O = red, N = blue, C = grey. Counter-anions, solvate molecules and H-atoms have been omitted for clarity.

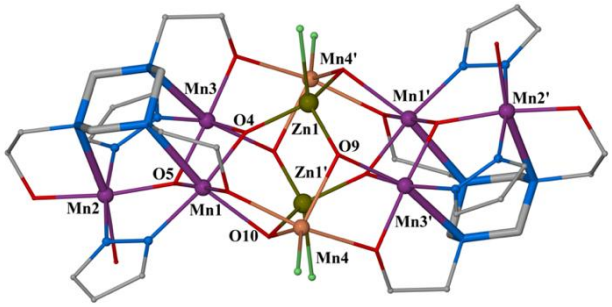

Figure 3. The crystal structure of complex **2**, highlighting the capping mode of the triaza N-atoms on the JT sites of Mn^{III} ions. Colour code: Mn^{III} = purple, Mn^{II} = orange, Zn= grey-green, O = red, N = blue, Br= green, C = grey. H-atoms are not displayed for clarity.

Complex $[Mn^{III}_6Mn^{II}_2Zn^{II}_4(L)_2(pyr)_6O_4(OH)_4Br_6(H_2O)_4]$ (**3**) (Figure 4, top) crystallizes in the monoclinic space group $P2_1/n$ with half the complex in the asymmetric unit (ASU). The analogous central hexagonal-bipyramidal $\{Mn^{III}_4Mn^{II}_2Zn^{II}_2\}$ core is again present, as in **1** and **2**, but it is now connected to two peripheral $\{Mn^{III}Zn^{II}\}$ units instead of the two Mn^{III} ions in **1** and **2**. This is facilitated by the presence of an additional pyr ligand (per ASU) and a change in the bridging mode of the ligand in which the previously terminally bound O-atom in **1** and **2** is μ-bridging.

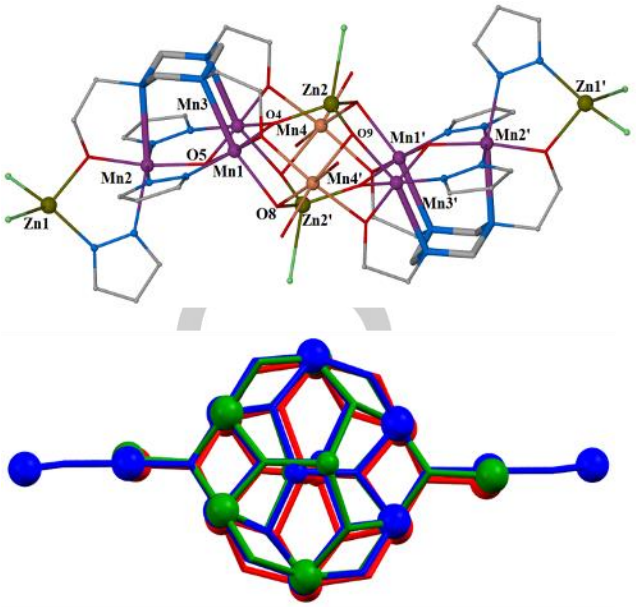

Figure 4. (Top) The molecular structure of **3**. Color code: Mn^{III} = purple, Mn^{II} = orange, Zn= grey-green, O = red, N = blue, Br= green, C = grey. H-atoms and THF solvate molecules are omitted for clarity. (Bottom) Overlay of the metallic cores of **1**-**3**. Colour code: Complex **1** = red, complex **2** = green, complex **3** = blue.

BVS calculations (Table S2) establish the same mixed-valent $\{Mn^{III}_6Mn^{II}_2\}$ oxidation state, with Mn4 (and s.e.) in the 2+ oxidation state. All Mn ions are six-coordinate, while all four Zn ions adopt tetrahedral geometry. The THF molecules of crystallization are H-bonded to the H_2O (O6, O7) molecules bonded to Mn5 (and s.e.; O(H)···O, ~2.7 Å) and to the μ_3-OH^- ion bridging between Mn1, Mn5 and Zn2 (O(H)···O, ~2.97 Å). There are no significant inter-clusters interactions, with the closest contacts being between the Br ions on one molecule and the L carbon atoms of its neighbour at ~ 3.8Å. The similarity between the structures of **1**-**3** is clearly evidenced by looking at the overlay diagram of the metallic skeletons of the three molecules shown in Figure 4 (bottom), in which little deviation between clusters is observed.

Direct current (dc) molar magnetic susceptibility measurements, χ_M, were performed on polycrystalline samples of complexes 1-3 in the T = 2 – 300 K temperature range under an applied field of B = 0.1 T, with the results plotted as the $\chi_M T$ product vs. T in Figure 5. The purity of the bulk crystalline material was established by means of: i) PXRD comparison between the experimental data and the simulated data from the single-crystal structure (Fig. S2) and ii) energy-dispersive spectroscopy (EDS) measurements (Fig. S3). From inspection of Figure 5 it is clear that all three complexes display similar behaviour which can be attributed to the $\{Mn^{III}_6Mn^{II}_2\}$ metallic core present in all three compounds: i) in the high temperature regime the $\chi_M T$ product for all three complexes decreases steadily upon cooling from 300-50 K, ii) in the ~50-20 K temperature range a plateau is observed, and iii) below ~20 K a rapid decrease in the $\chi_M T$ product is observed. More specifically, the room temperature $\chi_M T$ values of 21.2, 21.0 and 22.4 $cm^3\,K\,mol^{-1}$ for **1**-**3**, respectively, are lower than the value of 26.75 $cm^3\,K\,mol^{-1}$ expected for six Mn^{III} and two Mn^{II} non-interacting centers (g = 2.00), consistent with intramolecular antiferromagnetic exchange. Upon cooling to ~50 K, the $\chi_M T$ products decrease to 15.4 (**1**), 12.7 (**2**) and 17.0 (**3**)

cm^3 K mol^{-1}. The value then plateaus between ~50-20 K, and upon further cooling, the $\chi_M T$ products decrease rapidly to reach minimum values of 12.3 (**1**), 5.3 (**2**) and 9.6 (**3**) cm^3 K mol^{-1}. This is indicative of the presence of competing exchange interactions, with a predominance of nearest neighbour antiferromagnetic exchange. Differences in the susceptibility in **1**-**3** can be attributed to small differences in geometries, bond angles, bond distances and packing in the extended structure.

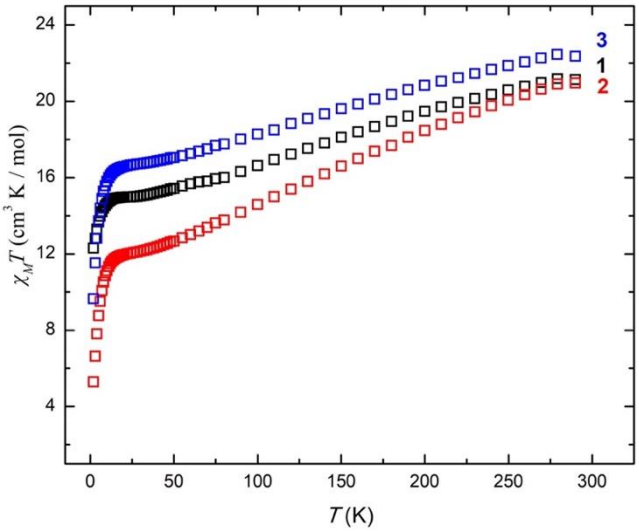

Figure 5. Plot of $\chi_M T$ *vs. T* for complexes **1**-**3** under an applied dc field of 0.1 T.

Low-temperature variable-temperature and variable-field magnetization data collected in the 2 - 6 K temperature range in magnetic fields up to 7 T are in agreement with this picture, with *M* rising only slowly with increasing *B* (Figure 6). At the lowest temperatures and highest fields measured, *M* reaches values of ~17.3, ~13.6 and 20.4 μ_B for **1**, **2**, and **3**, respectively. The data in each case suggests the presence of low-lying excited states with *S* values larger than the ground state, which are populated with increasing field due to Zeeman splitting. Furthermore, no frequency dependent out-of-phase signals were observed in the 1-1000 Hz and 2-40 K temperature range, even in the presence of an applied dc field.

The large nuclearity of the three compounds, presence of multiple exchange interactions and the anisotropy associated with the Mn^{III} ions precludes a quantitative analysis of the data. However, the data is entirely consistent with previous magneto-structural correlations of alkoxide-bridged [Mn^{III}_2] dimers with parallel JT axes oriented perpendicular to the bridging plane (Type I dimers) and to studies of mixed-valent [$Mn^{II}Mn^{III}$] dimers and butterflies which show that the exchange is weak and borderline ferro-/antiferromagnetic.[19-22]

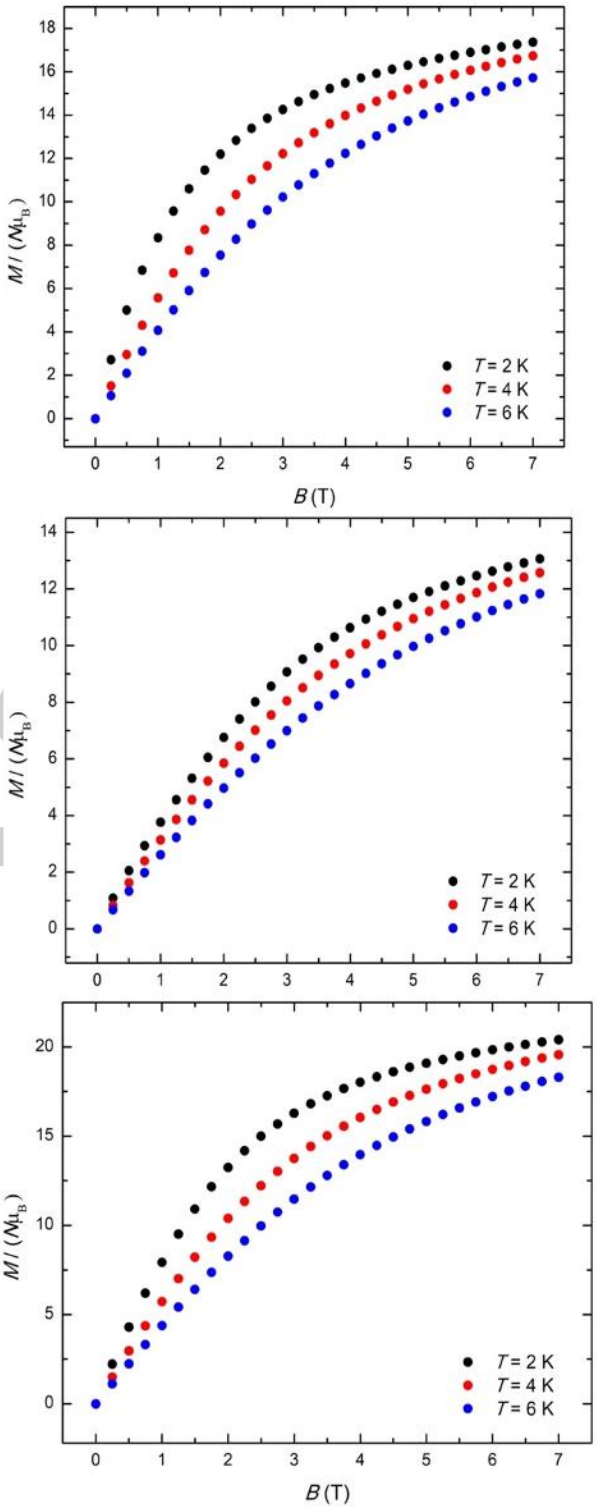

Figure 6. Isothermal molar magnetization *M* versus applied magnetic field data for **1** (top), **2** (middle), and **3** (bottom) collected at *T* = 2, 4 and 6 K.

Conclusion

Employment of the 1,3,5-tri(2-hydroxyethyl)-1,3,5-triazacyclohexane (H_3L) ligand in mixed-metal Mn/Zn chemistry in the presence of the auxiliary pyrazolate ligand led to the synthesis and isolation of the three closely-related clusters $[Mn^{III}_6Mn^{II}_2Zn^{II}_2(L)_2(pyr)_4O_4(OH)_4(NO_3)_2(MeOH)_2(H_2O)_4](NO_3)_2$.

H_2O (**1**·H_2O), $[Mn^{III}_6Mn^{II}_2Zn^{II}_2(L)_2(pyr)_4O_4(OH)_4Br_4(H_2O)_2]$ (**2**) and $[Mn^{III}_6Mn^{II}_2Zn^{II}_4(L)_2(pyr)_6O_4(OH)_4Br_6(H_2O)_4]$·8THF (**3**·8THF), all of which display similar structures based on hexagonal bipyramids. An important characteristic feature is that in all three clusters reported the ligand assembles an oxo-centered triangular $[Mn^{III}_3O(L)]^{4+}$ unit in which the triaza N-atoms favour coordination on the Jahn-Teller (JT) axes of the Mn^{III} ions leading to co-parallel alignment of the JT axes in the species; a feature that may prove of great significance for the control of the magnetic properties of the clusters as a means of introducing magnetic anisotropy in the species.

Experimental Section

Materials and physical measurements

All manipulations were performed under aerobic conditions, using solvents and materials as received from commercial sources without further treatment/purification. The ligand LH_3 was prepared following the published procedure.[2] Elemental analyses (C, H, N) were performed by the University of Ioannina microanalysis service. Solid state magnetic measurements were carried out on a Quantum Design SQUID MPMS 3 magnetometer equipped with a 7 T dc magnet at the University of Glasgow. Diamagnetic corrections were applied to the observed paramagnetic susceptibilities using Pascal's constants. Powder XRD measurements were performed on freshly prepared samples on a PANanalytical X'Pert Pro MPD diffractometer (UoC). Energy-dispersive X-ray Spectroscopy (EDS) measurements were performed on a JEOL Scanning Electron Microscope (UoC).

Synthesis of $[Mn^{III}_6Mn^{II}_2Zn^{II}_2(L)_2(pyr)_4O_4(OH)_4(NO_3)_2(MeOH)_2(H_2O)_4](NO_3)_2{\cdot}H_2O$ (1·H_2O). $Mn(NO_3)_2{\cdot}6H_2O$ (143 mg, 0.5 mmol), $Zn(NO_3)_3{\cdot}6H_2O$ (149 mg, 0.5 mmol), LH_3 (109 mg, 0.5 mmol), pyrazole (34 mg, 0.5 mmol) and NEt_3 (1.5 mmol) were added to MeOH (20 mL), and the resultant yellow-orange solution kept under stirring for 60 minutes to form a dark brown solution. The solution was then filtered and left undisturbed to evaporate slowly at room temperature, forming dark-brown crystals of **1** after 3 days in ~35% yield. The crystals were collected by filtration, washed with Et_2O (2 x 5 ml) and dried in air. Anal. calcd. for $C_{32}H_{56}Mn_8N_{17}O_{30}Zn_2$ (**1**·H_2O): C, 22.23; H, 3.26; N, 13.77%. Found: C, 22.11; H, 3.05; N 13.68%. Main IR data (ATR-FTIR): *v*= 1495m, 1366s, 1273s, 1176s, 1075s, 1044vs, 943vs, 760s, 621vs.

Synthesis of $[Mn^{III}_6Mn^{II}_2Zn^{II}_2(L)_2(pyr)_4O_4(OH)_4Br_4(H_2O)_2]$ (2). Complex **2** was prepared in an analogous manner to **1**, using $MnBr_2{\cdot}4H_2O$ instead of $Mn(NO_3)_2{\cdot}6H_2O$. Dark-brown crystals suitable for X-ray diffraction were formed after 4 days in ~30% yield. Anal. calcd. for $C_{30}H_{48}Br_4Mn_8N_{14}O_{16}Zn_2$ (**2**): C, 20.58; H, 2.76; N, 11.20%. Found: C, 20.53; H, 2.66; N 11.14%. Main IR data (ATR-FTIR): *v*= 1491m, 1362s, 1277s, 1176s, 1075s, 1044vs, 951vs, 760vs, 628vs.

Synthesis of $[Mn^{III}_6Mn^{II}_2Zn^{II}_4(L)_2(pyr)_6O_4(OH)_4Br_6(H_2O)_4]$·8THF (3·8THF). Complex **3** was prepared in the same manner as **2**, but using a mixture of solvents MeOH/THF (1:1, 20 mL). Dark-brown crystals formed after 3 days in ~35% yield. Anal. calcd. for $C_{48}H_{90}Br_6Mn_8N_{18}O_{21}Zn_4$ (**3**·3THF): C, 23.67; H, 3.72; N, 10.35%. Found: C, 23.79; H, 3.59; N 10.21%. Main IR data (ATR-FTIR): *v*= 1495vs, 1370vs, 1281s, 1176s, 1087s, 1039vs, 954vs, 861m, 741s, 648s, 621vs, 586vs.

X-ray Crystallography and Structure Solution.

Diffraction data for **1** - **3** were collected on a Bruker D8 VENTURE diffractometer (University of Crete), equipped with a PHOTION II CPAD detector. Data collection parameters and structure solution and refinement details are listed in Table S1. Full details can be found in the CIF files with CCDC reference numbers 2174252 (for **1**), 2174253 (for **2**) and 2174254 (for **3**).

Acknowledgements

CJM and TGT thank the Hellenic Foundation for Research and Innovation (H.F.R.I.) under the "First Call for H.F.R.I. Research Projects to support Faculty members and Researchers and the procurement of high-cost research equipment grant" (Project Number: 400). EKB thanks the EPSRC for financial support under grant reference number EP/V010573/1. M.M. thanks the University of Glasgow for financial support.

Conflict of interest

The authors declare no conflict of interest

Data Availability Statement

The data that support the findings of this study are available from the corresponding author upon reasonable request.

Keywords: manganese • zinc • heterometallic clusters • 1,3,5-tri(2-hydroxyethyl)-1,3,5-triazacyclohexane • magnetic properties

[1] See for example: A. J. Tasiopoulos, S. P. Perlepes, *Dalton Trans.* **2008**, 5537-5555.
[2] M. V. Baker, D. H. Brown, B. W. Skelton, H. White, *J. Chem. Soc. Dalton Trans.* **1999**, 1483-1490.
[3] M. Riaz, R. K. Gupta, H. -F. Su, Z. Jagličić, M. Kurmoo, C. -H. Tung, D. Sun, L. -S. Zheng, *Inorg. Chem.* **2019**, *58*, 14331-14337.
[4] T. G. Tziotzi, M. Coletta, M. Gray, C. L. Campbell, S. J. Dalgarno, G. Lorusso, M. Evangelisti, E. K. Brechin, C. J. Milios, *Inorg. Chem. Front.* **2021**, *8*, 1804-1809.
[5] M. Coletta, T. G. Tziotzi, M. Gray, G. S. Nichol, M. K. Singh, C. J. Milios, E. K. Brechin, *Chem. Commun*. **2021**, *57*, 4122-4125.
[6] J. Schnack, *Dalton Trans*. **2010**, *39*, 4677-4686.
[7] R. Inglis, C. J. Milios, L. F. Jones, S. Piligkos, E. K. Brechin, *Chem. Commun*. **2012**, *48*, 181-190.
[8] P. Comar, T. Rajeshkumar, G. S. Nichol, M. B. Pitak, S. J. Coles, G. Rajaraman, E. K. Brechin, *Dalton Trans*. **2015**, *44*, 19805-19811.
[9] W. P. Barros, R. Inglis, G. S. Nichol, T. Rajeshkumar, G. Rajaraman, S. Piligkos, H. O. Stumpf, E. K. Brechin, *Dalton Trans*. **2013**, *42*, 16510-16517.
[10] N. Berg, T. Rajeshkumar, S. M. Taylor, E. K. Brechin, G. Rajaraman, L. F. Jones, *Chem. – Eur. J.* **2012**, *18*, 5906-5918.
[11] R. Inglis, E. Houton, J. Liu, A. Prescimone, J. Cano, S. Piligkos, S. Hill, L. F. Jones, E. K. Brechin, *Dalton Trans*. **2011**, *40*, 9999-10006.
[12] T. Tanase, S. P. Watton, S. J. Lippard, *J. Am. Chem. Soc*. **1994**, *116*, 9401-9402.
[13] W. Clegg, I. R. Little, B. P. Straughan, *Inorg. Chem*. **1988**, *27*, 1916-1923.
[14] Y. Sunatsuki, H. Shimada, T. Matsuo, M. Nakamura, F. Kai, N. Matsumoto, N. Re, *Inorg. Chem*. **1998**, *37*, 5566-5574.
[15] P. L. Feng, C. C. Beedle, W. Wernsdorfer, C. Koo, M. Nakano, S. Hill, D. N. Hendrickson, *Inorg. Chem*. **2007**, *46*, 8126-8128.
[16] E. Y. Tsui, R. Tran, J. Yano, T. Agapie, *Nature Chem*. **2013**, *5*, 293-299.

[17] C. Tan, J. Jiao, Z. Li, Y. Liu, X. Han, Y. Cui, *Angew. Chem., Int. Ed.* **2018**, *57*, 2085-2090.

[18] B. C. Khadka, A. Eichhöfer, F. Weigend, F. J. Corrigan, *Inorg. Chem.* **2012**, *51*, 2747-2756.

[19] N. Berg, T. Rajeshkumar, S. M. Taylor, E. K. Brechin, G. Rajaraman, L. F. Jones, *Chem. Eur. J.* **2012**, *18*, 5906-5918.

[20] S. M. Taylor, G. Karotsis, R. D. McIntosh, S. Kennedy, S. J. Teat, C. M. Beavers, W. Wernsdorfer, S. Piligkos, S. J. Dalgarno, E. K. Brechin, *Chem. Eur. J.* **2011**, *17*, 7521-7530.

[21] K. R. Vignesh, S. K. Langley, C. J. Gartshore, I. Borilović, C. M. Forsyth, G. Rajaraman, K. S. Murray, *Dalton Trans*. **2018**, *47*, 11820-11833.

[22] K. R. Vignesh, S. K. Langley, C. J. Gartshore, B. Moubaraki, K. S. Murray, G. Rajaraman, *Inorg. Chem.* **2017**, *56*, 1932-1949.

Entry for the Table of Contents

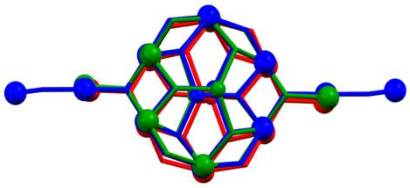

The use of the 1,3,5-tri(2-hydroxyethyl)-1,3,5-triazacyclohexane ligand in mixed-metal manganese/zinc chemistry leads to the synthesis of three closely-related complexes; two decanuclear $\{Mn^{III}_6Mn^{II}_2Zn^{II}_2\}$ and one dodecanuclear $\{Mn^{III}_6Mn^{II}_2Zn^{II}_4\}$ clusters, all of which display similar structures based on a hexagonal-bipyramidal $\{Mn_6Zn_2\}$ central unit.